

# Magnetotransport in a double quantum wire: Modeling using a scattering formalism built on the Lippmann-Schwinger equation

Vidar Gudmundsson<sup>1</sup> and Chi-Shung Tang<sup>2</sup>

<sup>1</sup>Science Institute, University of Iceland, Dunhaga 3, IS-107 Reykjavik, Iceland

<sup>2</sup>Physics Division, National Center for Theoretical Sciences, P.O. Box 2-131, Hsinchu 30013, Taiwan

We model electronic transport through a double quantum wire in an external homogeneous perpendicular magnetic field using a scattering formalism built on the Lippmann-Schwinger equation. In the scattering region a window is opened between the parallel wires allowing for inter- and intra-wire scattering processes. Due to the parity breaking of the magnetic field the ensuing subband energy spectrum of the double wire system with its regimes of hole- and electron-like propagating modes leads to a more structure rich conductance as a function of the energy of the incoming waves than is seen in a single parabolically confined quantum wire. The more complex structure of the evanescent modes of the system also leaves its marks on the conductance.

PACS numbers: 73.23.-b, 73.21.Hb, 85.35.Ds

## I. INTRODUCTION

We investigate coherent electronic transport in a ballistic double-quantum-wire (DQW) system. The electronic propagating modes in the two wires are allowed to be coupled through a window between the separated wires. Such a wave-function mixing can be enhanced in the presence of a perpendicular parity breaking magnetic field.

Earlier, discrete models of a single quantum wire with embedded island-like obstacles have been investigated by Gu et al. using a transfer matrix technique to describe the transport channels around the islands as two coupled chains.<sup>1</sup> A similar continuous model has been studied by Tang et al. in order to identify coupling modes between the channels.<sup>2</sup> The question still remains how would the transport be in a double wire system where the electron waves enter the scattering region already in eigenstates of the double wire.

In the presence of the perpendicular magnetic field the energy spectrum of pure double quantum wire homogeneous in the long direction has been investigated by Barbosa and Butcher pointing out the especially complex structure of the evanescent states of the system.<sup>3</sup> The properties of the energy spectrum of a double wire system in a magnetic field has also been addressed by Koropov and Liberman who calculate the effects of a single delta impurity or disorder and boundary roughness in a weakly coupled system of quantum wires.<sup>4,5</sup>

We have used the methodology of Gurvitz<sup>6</sup> to solve the Lippmann-Schwinger equation for a single parabolic quantum wire in an external perpendicular magnetic field in a momentum-coordinate space, transforming the 2D-equation into a coupled set of 1D integral equations, one for each incoming transport mode.<sup>7</sup> In this paper we use the eigenfunctions of the parabolically confined single quantum wire in a magnetic field as a basis to expand the more complex wave functions of a double wire system in, and thus again arrive at a coupled set of 1D integral equations for the  $T$ -matrix that we then subsequently use to extract information about the conductance from accord-

ing to the Landauer-Büttiker formalism, or the electronic probability density of the system.<sup>7</sup> We are thus able to handle a system of weakly or strongly coupled quantum wires of a wide variety of shapes.

## II. MODEL

We consider a quantum wire extended homogeneously in the  $x$ -direction, but the confinement in the  $y$ -direction is governed by

$$V_{\text{conf}}(y) = \frac{1}{2}m^*\Omega_0^2y^2 + V_\delta(y)D + E_{00}, \quad (1)$$

with a symmetric deviation from the parabolic confinement

$$\begin{aligned} V_\delta(y) = & -V_{d_1} \exp(-\beta_1(y - y_0)^2) \\ & + V_{d_0} \exp(-\beta_0 y^2) \\ & - V_{d_1} \exp(-\beta_1(y + y_0)^2). \end{aligned} \quad (2)$$

The dimensionless parameter  $D$  takes values in the interval  $[0, 1]$  and controls the overall strength of the modulation of the double quantum wire. The scattering potential is of the type

$$V_{\text{sc}}(x, y) = V_0 \exp(-\alpha x^2 - \beta_0 y^2), \quad (3)$$

and with the choice  $V_0 = -V_{d_0}$  can be made to represent a window between the parallel wires as is shown in Fig. 1 for the parameters:  $V_{d_1} = 6.0$  meV,  $V_{d_0} = -V_0 = 2.0$  meV,  $\hbar\Omega_0 = 1.0$  meV,  $\beta_0 = 4.0 \times 10^{-3}$  nm $^{-2}$ ,  $\alpha = 0.2 \times 10^{-3}$  nm $^{-2}$ ,  $\beta_1 = 0.7 \times 10^{-3}$  nm $^{-2}$ , and  $y_0 = 100$  nm.  $E_{00} = 2.0$  meV is a convenient zero point to avoid negative energy in the potential. In the case of a parabolically confined quantum wire in perpendicular magnetic field we have used the approach of Gurvitz using a mixed momentum-coordinate representation<sup>6</sup> of the wave functions

$$\Psi_E(q, y) = \sum_n \varphi_n(q) \phi_n(q, y), \quad (4)$$

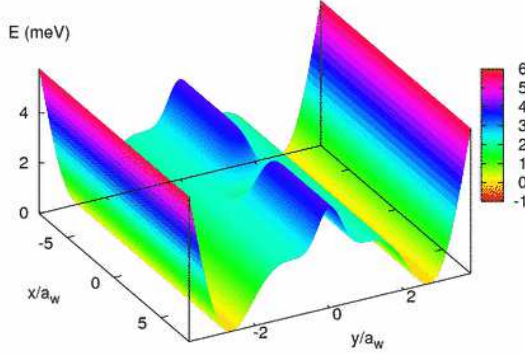


FIG. 1: (Color online) A section of the double quantum wire showing the scattering potential, the window between the wires. The color scale on the right shows the potential height in meV. The effective magnetic confinement length  $a_w = 33.7$  nm, and other parameters are in the text.

in order to reduce the two-dimensional Lippmann-Schwinger equation into a coupled set of one-dimensional integral equations for the T-matrix,<sup>7</sup> where  $\phi_n$  is an eigenfunction for the parabolic wire in the presence of the magnetic field. Now we use the expansion

$$\Psi_E(q, y) = \sum_n \varphi_n(q) \Phi_n(q, y), \quad (5)$$

with the eigenfunctions  $\Phi_n(q, y)$  of the new double wire confinement Eq. (1) expanded in the basis for the parabolic confinement

$$\Phi_n(q, y) = \sum_n c_{nm}(q) \phi_m(q, y). \quad (6)$$

The coefficients  $c_{nm}(q)$  are found by diagonalizing the corresponding Hamiltonian in each  $q$ -subspace separately. In this approach the momentum or the Fourier variable  $q$  takes over the role of the “center-coordinate”  $y_0$  but loosens up the strict connection between the center-coordinate and the momentum of the electron required by the magnetic field. The Lippmann-Schwinger equation is separable in the  $(q, y)$ -space but is not so in the  $(x, y)$ -space due to the Lorentz force.<sup>6,7</sup>

This diagonalization of the Hamiltonian for the pure wire without an embedded scattering center supplies the energy bands  $E_n(q)$  for the propagating states (when  $q$  is real) in the asymptotic regions of the double wire

$$E_n(q) = E_n^0 + \epsilon(n, q) + \frac{(qa_w)^2}{2} \frac{(\hbar\Omega_0)^2}{\hbar\Omega_w} \quad (7)$$

with  $E_n^0 = \hbar\Omega_w(n + 1/2)$ . The effective confinement frequency  $\Omega_w$  and the effective magnetic length  $a_w$  are connected through

$$a_w^2 = \frac{\hbar}{m^*} \frac{1}{\Omega_w} = \frac{\hbar}{m^*} \frac{1}{\sqrt{\Omega_0^2 + \omega_c^2}}, \quad (8)$$

with  $\omega_c = eB/(m^*c)$  the cyclotron frequency. The energy  $\epsilon(n, q)$  is the correction to the spectrum of the parabolic wire due to the deviation from the parabolic confinement (2). Its dependence on the band index  $n$  makes the subbands generally not equidistant in energy.

In the open quasi-one-dimensional system considered here we are studying elastic scattering of the electrons. The incoming and outgoing states have thus the same definite energy  $E$  in the asymptotic regions of the wire. The Lippmann-Schwinger equation includes all virtual energy-nonconserving transitions in the scattering region. A virtual state can be a bound state, a propagating one, or a quasi-bound state. Evanescent states are localized quasi-bound states with finite life time. The subband structure of the energy spectrum of the wire embeds them into the energy continuum making them essential in order to obtain the correct conductance of the system, especially when the energy of the incoming electrons is close to a subband bottom.

In order to calculate the energy of the evanescent states (with  $q$  imaginary) we can not use a procedure similar to the one we used to evaluate the energy spectrum of the propagating states. The evanescent states are not orthogonal and the resulting generalized eigenvalue problem is almost singular except for  $q \approx i0^+$ . An observation of the character of evanescent wave functions for the parabolic confinement explains these difficulties. An evanescent wave function is always centered around the middle of the wire,  $y = 0$ , and develops a high number of nodes as  $q$  assumes a higher imaginary value. On the other hand a propagating state has a wave function that shifts along the  $y$ -direction as  $q$  is changed and its number of nodes correlates to the quantum number  $n$ . Our solution is thus to expand the evanescent states in terms of the eigenfunctions of the parabolic wire at zero magnetic field, but using in them the effective magnetic length for  $B \neq 0$

$$\phi_n^0(y) = \frac{\exp\left(-\frac{y^2}{2a_w}\right)}{\sqrt{2^n \sqrt{\pi} n! a_w}} H_n\left(\frac{y}{a_w}\right). \quad (9)$$

The complete basis (9) thus used for the expansion of the evanescent states is composed of wave functions that are all centered around  $y = 0$  as are the evanescent wave functions for a parabolically confined wire. In the numerical calculations the truncation of the bases  $\{\phi_n^0(y)\}$  and  $\{\phi_n^0(q, y)\}$  is not performed for the same  $n$ . The character of the evanescent wave functions requires a much larger basis for their expansion.

With the basis (9) and an imaginary  $q$  to find the energy spectrum of the evanescent states the effective Hamiltonian matrix with the confinement potential (1) but without the scattering potential (3) we need to diagonalize is non-Hermitian as long as  $\omega_c \neq 0$ . The evanescent modes have real eigenvalues when they are not degenerate, but they have an imaginary part when they are degenerate. We assume this reflects the fact that the wave vectors of the evanescent modes can be complex

when the states are calculated explicitly without using the basis (9) we use.<sup>5</sup> We find the real part of our energy spectrum for the evanescent modes to be consistent with the results of Barbosa and Butcher<sup>3</sup> and Korepov and Libermann<sup>5</sup> for nonparabolic confinement. We thus discard the imaginary part of the energy spectrum for the evanescent modes found by our method.

The electron scattering in the wire is elastic. For the parabolic wire this means that an electron with energy  $E$  in the asymptotic free region would have a subband momentum  $\pm k_n(E)$  if it could propagate in the subband with index  $n$ . The deviation from the parabolic confinement requires the subband momentum in subband  $n$  to be found from the condition

$$[k_n(E)a_w]^2 = 2 [E - E_n^0 - \epsilon(n, q)] \frac{\hbar\Omega_w}{(\hbar\Omega_0)^2}. \quad (10)$$

For the more complicated confinement assumed here each subband can support more than one or two propagating states. These different transport modes correspond to the poles,  $q_{n_i}$ , of the scattering Green function

$$G_E^n(q) = \frac{1}{(k_n(E)a_w)^2 - (qa_w)^2 + i0^+}, \quad (11)$$

and are located where the incoming energy  $E$  intersects the energy subband  $n$ . The index  $i$  labels the modes in subband  $n$  in the direction of increasing  $q$ . The energy spectrum of the evanescent states enters the Green function for the subbands with no propagating modes present, i.e. for subbands with threshold energy higher than  $E$ .<sup>8,9</sup>

The resulting coupled one-dimensional Lippmann-Schwinger equations for the transport modes supply the T-matrix and the probability amplitudes for transmission in mode  $n_i$  with momentum  $\hbar k_{n_i}$  if the in-state is in mode  $m_j$  with momentum  $\hbar k_{m_j}$

$$t_{n_i m_j}(E) = \delta_{n_i m_j} - \frac{i\sqrt{(k_{m_j}/k_{n_i})}}{2(k_{m_j}a_w)} \left( \frac{\hbar\Omega_0}{\hbar\Omega_w} \right)^2 \times \tilde{T}_{n_i m_j}(k_{n_i}, k_{m_j}). \quad (12)$$

The conductance is then according to the Landauer-Büttiker formalism defined as

$$G(E) = \frac{2e^2}{h} \text{Tr}[\mathbf{t}^\dagger(E)\mathbf{t}(E)], \quad (13)$$

where  $\mathbf{t}$  is evaluated at the Fermi energy.

### III. RESULTS AND DISCUSSION

In order to understand the conductance of the double wire system we can correlate it to the energy spectrum in the asymptotic region far away from the scattering region in the middle of the wire. To further clarify the conductance for a certain incoming energy of the electrons we will seek information from the electron probability density of the various modes active at that point. We assume GaAs parameters here with  $m^* = 0.067m_e$ .

Figures 2 and 3 present some general features of the energy spectra at a vanishing magnetic field and at a finite one. In Figure 2 the energy spectrum for  $B = 0$  is shown for three different strengths of modulation of the wire shape.  $D = 0$  corresponds to a parabolic confinement and the energy spectrum in Fig. 2(a) displays the familiar spectrum of a parabolic quantum wire in vanishing magnetic field. We only show here 7 of each of the 9 propagating and 9 evanescent subbands included in the present calculation. The shape of the wire deter-

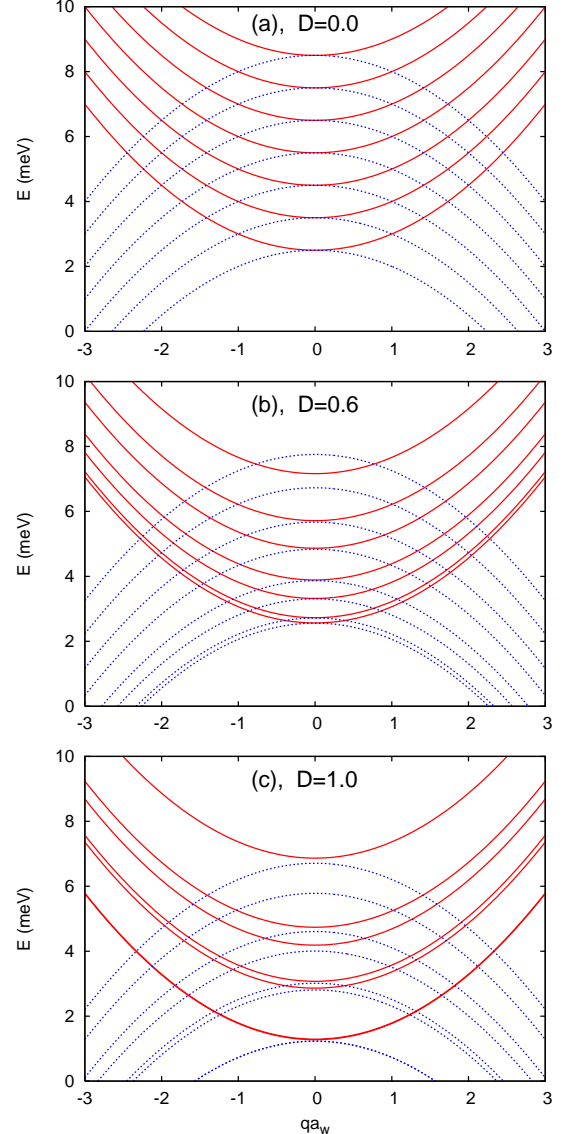


FIG. 2: (Color online) The energy spectrum of the propagating electronic states (solid red) vs. the Fourier parameter  $q$ , and the energy spectrum of the evanescent states (dotted blue) vs.  $iq$ , in the asymptotically free regions of the quantum wire.  $D$  is an overall multiplicative factor to the deviation  $V_\delta(y)$  from the parabolic confinement.  $B = 0$  T.

mined by Eq.'s (1) and (2) is always symmetric around its center line  $y = 0$  requiring the wave functions to be

either symmetric or antisymmetric in the case of no magnetic field. The resulting energy subbands are parabolic and have their bottom (or top in case of the evanescent ones) at  $q = 0$  but are not equidistant any more since the deviation from the parabolic confinement (2) shifts the subbands to a different extend depending on their parity. For  $D = 0$  in Fig. 2(a) the energy gap between the two lowest subbands  $\Delta_{01} = \hbar\Omega_w = 1.0$  meV at  $q = 0$ . In Fig. 2(b) the lowest propagating subband representing symmetric wave functions is shifted up in energy very close to the next subband of antisymmetric wave functions and  $\Delta_{01} = 0.16$  meV. In Fig. 2(c) the stronger parabolic deviation causes a near accidental degeneration between these two lowest subbands and higher subbands appear to come in pairs,  $\Delta_{01} = 0.017$  meV.

The magnetic field changes the character of the energy spectrum as can be seen in Fig. 3 by destroying the parity of the wave functions. Physically this can be related to the action of the Lorentz force that pushes the electrons away from the center of the wire in ratio to their momentum along the wire. In a parabolic wire only the energy separation of the subbands is renormalized by the magnetic field (Fig. 3(a)) with  $\Delta_{01} = 1.32$  meV, but in a double wire the minimum of a propagating energy subband does not have to be at  $q = 0$ . The evanescent subbands assume a complex form that has been detailed by Barbosa and Butcher.<sup>3</sup> In Figure 3(b) with  $\Delta_{01} = 0.66$  meV and in subfigure 3(c) we notice that states with a finite “subband momentum”  $q$  can be off-centered by the Lorentz force enough to occupy mostly only one of the parallel wires and thus acquiring less potential energy leading to a minimum total energy at  $q \neq 0$ . In addition, we see in Figure 3(c) that the value  $D = 1$  leads to energy subbands formed by a strong admixture of several subbands for the parabolic wire,  $\Delta_{01} = 0.16$  meV.

We now turn to analysis of the conduction properties of the double wire system in an external magnetic field with the help of the energy spectra for the asymptotic regions of the wire. The scattering potential (3) creates a shallow window between the parallel wires as is displayed in Fig. 1. In the case of an ideal parabolic wire the conductance increased monotonically step wise as a function of  $E$ , with a new step appearing at the onset of each new propagating subband. For an ideal double wire system the steps do not increase monotonically with increasing  $E$ , but instead reflect the much richer subband structure of the system.

Figure 4 presents the conductance for the system with the modulation of the parabolic deviation of the wire shape  $D = 0.6$  and the same reduction applies to the scattering potential (3). Shortly after the energy of the incoming electrons hits the lowest subband bottom the conductance jumps to  $2G_0$  indicating two propagating modes. The two modes remain active with increasing in-energy  $E$  until the local maximum at  $q = 0$  is surpassed at  $E = 3.03$  meV and the conductance falls to  $G_0$  as only one incoming mode is active. Between the global minimum and the local maximum of the subband at  $q = 0$

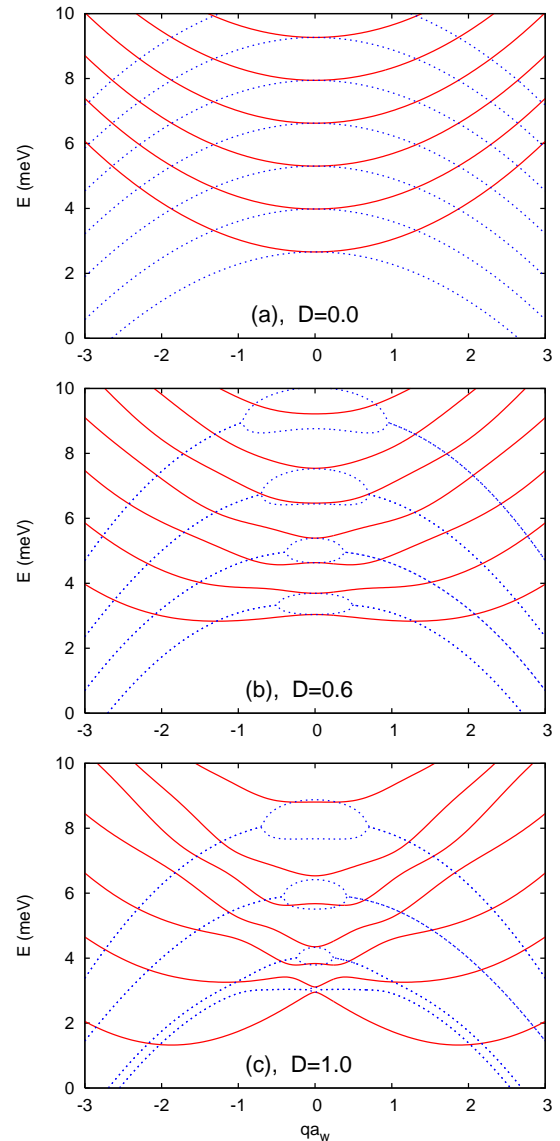


FIG. 3: (Color online) The energy spectrum of the propagating electronic states (solid red) vs. the Fourier parameter  $q$ , and the energy spectrum of the evanescent states (dotted blue) vs.  $iq$ , in the asymptotically free regions of the quantum wire.  $D$  is an overall multiplicative factor to the deviation  $V_\delta(y)$  from the parabolic confinement.  $B = 0.5$  T.

the conductance of the system goes through a minimum close to the point of inflection separating the states of the subband that are hole-like close to  $q \approx 0$  and electron like nearer the global minimum. For  $E$  below the inflection point the incoming electron states travel very close to the center barrier between the wires, and in addition the Lorentz force pushes them towards the barrier. In the scattering region, in the window, the Lorentz force manages (if the window is long enough compared with the magnetic length) to push the electron wave partially into the barrier region. Part of the wave is thus reflected and a part tunnels within the central barrier before emerging

again as a traveling wave close to the central barrier. The tunneling distance can be quite considerable as we shall show in a figure in combination with the discussion about the transport in a wire with a stronger double wire modulation ( $D = 1$ ). The hole-like states with  $E$  higher than the inflection point do experience the Lorentz force that pulls them away from the barrier. In the window region they are thus less likely to be reflected and the conductance rises again. The effectiveness of Lorentz force to shift the center of the states depends not only on their respective kinetic energy, but also on their effective mass which is singular at the point of inflection.

This distinction in the behavior of hole- or electron-like states can not be observed in a parabolic single quantum wire and in a double wire system the magnetic field perpendicular to the wire is essential.

In the semi-subband gap between  $E = 3.03$  and  $3.7$  meV the single outer mode goes undisturbed through the wire system as the Lorentz force steers it clear of the small window between the two parallel wires. Just

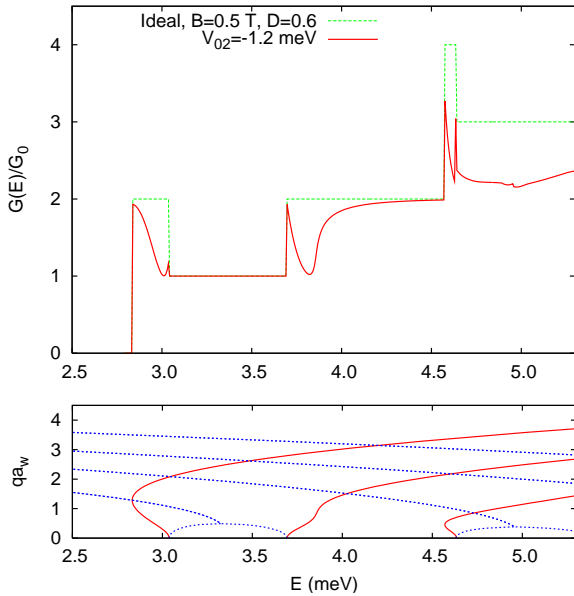


FIG. 4: (Color online) (Upper panel) The conductance of an ideal weakly ( $D = 0.6$ ) modulated double quantum wire without a window (dashed green), and with a window between the wires (solid red). (Lower panel) The energy spectrum of the propagating electronic states (solid red) vs. the Fourier parameter  $q$ , and the energy spectrum of the evanescent states (dotted blue) vs.  $iq$ , in the asymptotically free regions of the quantum wire.  $B = 0.5$  T,  $\alpha = 0.0002$  nm $^{-2}$ , and  $V_0 = -1.2$  meV.

above  $E = 3.7$  meV the second subband becomes active in the transport and the total conductance of the system reaches  $2G_0$ . At the bottom of this subband there is no local maximum at  $q = 0$  as in the first subband, but for a bit higher  $q$  the deviation from the parabolic shape of the system produces a point of inflection. Again the states near the bottom of the second subband reside close to

the small central barrier like those close to the bottom of the first subband. The main difference now being that their wave function have a double hump structure in the  $y$ -direction. The fine interplay of the Lorentz force and the window between the wires produces again a minimum of conductance around the point of inflection in a similar manner as occurred in the first subband. With increasing  $E$  the shape of the subband approaches a normal form for electronic states and the conductance rises slowly to  $2G_0$  since now states in both subbands at higher values of  $q$  steer clear of the window between the wires. With the activation of the third subband we see a similar structure in the conductance as observed at the beginning of the first subband, as these two subbands have a similar shape for low  $q$  values.

The conductance for the stronger modulated double quantum wire with  $D = 1$  is shown in Fig. 5 for three different lengths of the window between the parallel wires. The window length is controlled by the parameter  $\alpha$  introduced in the scattering potential in eq. (3). The value  $\alpha = 0.0002$  nm $^{-2}$  was used for the shape of the wire shown in Fig. 1 and in the conductance calculation for Fig. 4. Higher values of  $\alpha$  lead to a shorter window. The

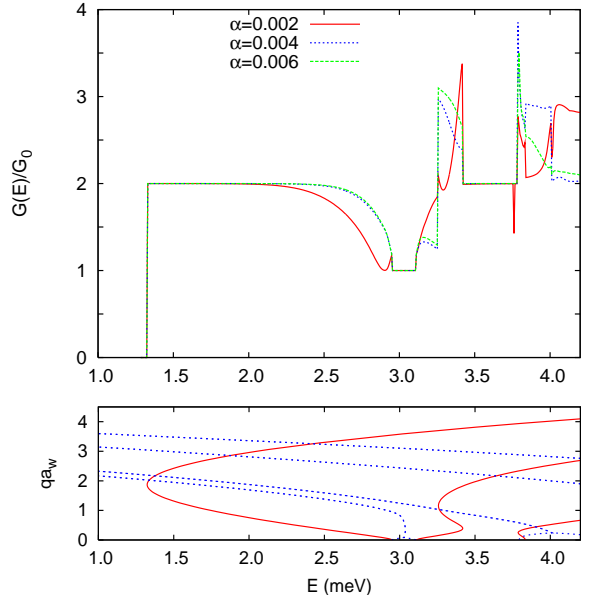


FIG. 5: (Color online) (Upper panel) The conductance of a double quantum wire with a window between the wires of different lengths indicated by the three different values of  $\alpha$  used for the scattering potential (3). (Lower panel) The energy spectrum of the propagating electronic states (solid red) vs. the Fourier parameter  $q$ , and the energy spectrum of the evanescent states (dotted blue) vs.  $iq$ , in the asymptotically free regions of the quantum wire.  $B = 0.5$  T,  $D = 1.0$ , and  $V_0 = -2.0$  meV.

conductance up to  $E = 2.95$  is in accordance with the results for the lowest subband in Fig. 4 caused by the fine tuned interplay of the Lorentz force and the window size and the character of the transport states. Here

we use the opportunity to clarify the effects through the probability distribution of the electrons. In Fig. 7 we display the probability density for three different values of  $E$  for the incoming state  $n_i = 0_2$ , in the double wire with the longer window with  $\alpha = 0.0002 \text{ nm}^{-2}$ , close to the conductance minimum at  $E = 2.902 \text{ meV}$  and the inflection point of the subband. The other active incoming transport mode ( $n_i = 0_4$ ) in this energy region passes the scattering region unperturbed and is therefore not shown here.

To make the subsequent discussion of transport modes clearer we have in Fig. 6 labeled the active transport modes for two different values of the incoming energy that are referred to later.

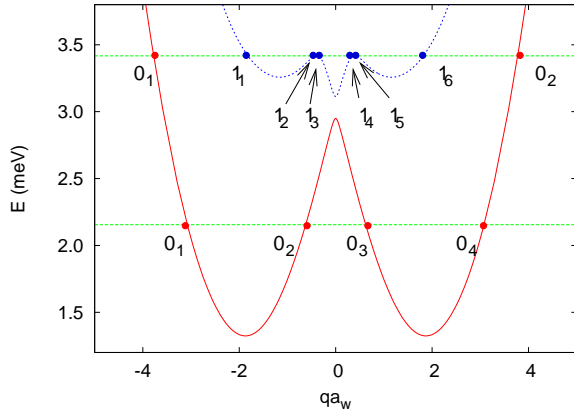


FIG. 6: (Color online) The energy spectrum of the two lowest propagating electronic subbands vs. the Fourier parameter  $q$  in the asymptotically free regions of the quantum wire. The two horizontal dashed green lines represent the energies  $E = 2.155 \text{ meV}$  and  $E = 3.417 \text{ meV}$ . The active transport modes are labeled for these two energies with the notation  $n_i$ , where  $i$  is the number of the active mode in subband number  $n$ .  $D = 1$  and  $B = 0.5 \text{ T}$ .

Well below the inflection point the electron-like in-state at  $E = 2.155 \text{ meV}$  depicted in Fig. 7(a) contributing  $0.98 \text{ G}_0$  to the total conductance enters the wire on the right side of the thin central barrier between the wires and is only slightly perturbed in the window region. In Fig. 7(b) corresponding to the conductance minimum at  $E = 2.902 \text{ meV}$  the wave is deflected into the window region causing the largest part of it to be backscattered and a small portion tunneling into the continuation of the central barrier on the other side of the window emerging as a traveling wave a good distance from the window. In case of a shorter window,  $\alpha \geq 0.0004 \text{ nm}^{-2}$ , the electron wave interacts to a lesser extent with the window and no clear distinction can be seen between the behavior of hole- or electron-like states. The shorter window is getting small on the scale of the magnetic length and can not effectively interfere with the wave with the help of the Lorentz force. The hole-like in-mode seen in Fig. 7(c) at  $E = 2.942 \text{ meV}$  avoids due to the opposite directed Lorentz force the strong backscattering in the window re-

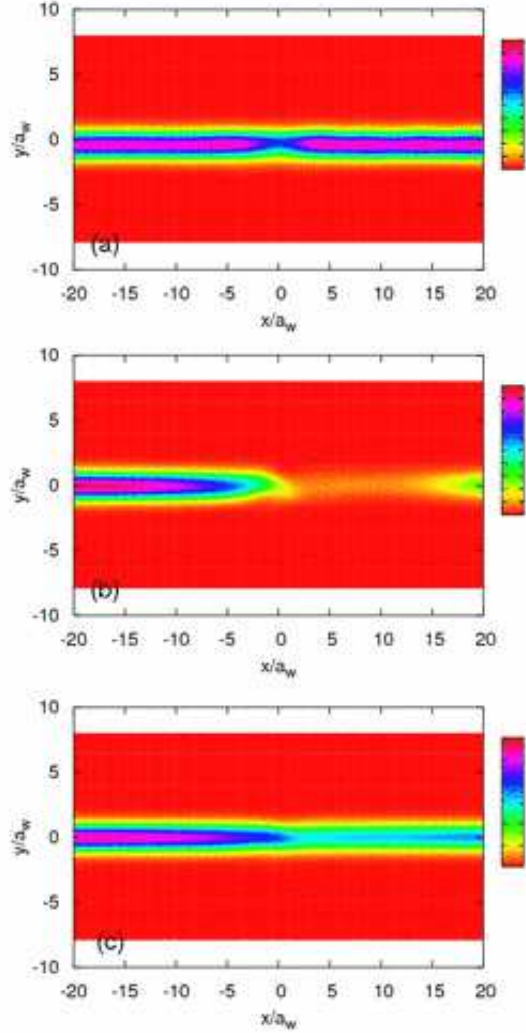


FIG. 7: (Color online) The electron probability density for the  $n_i = 0_2$  electron-like mode at input energy  $E = 2.155 \text{ meV}$  (a), for the mode at  $E = 2.902 \text{ meV}$  (b), and for the hole-like mode at  $E = 2.942 \text{ meV}$  (c).  $B = 0.5 \text{ T}$ ,  $\alpha = 0.0002 \text{ nm}^{-2}$ , and  $D = 1.0$  corresponding to the solid red curve in the upper panel of Fig. 5.

gion. The accuracy of these results has been checked by increasing all relevant grid or basis set sizes used in the numerical calculation. For the calculation here we have used 9 subbands, and divided the  $q$ -integration into three regions:  $qa_w \in (0, 3)$ ,  $(3, 7)$ , and  $(7, 10)$ . In each region we apply a repeated 4-point Gauss integration. For the calculation of the conductance we need 32 repetitions in the first interval, 24 in the second, and 8 in the last one. This is then mirrored for the negative values of  $q$ . For the probability density we double the density of the points, but use the same intervals.

In the semi-gap region  $2.95 < E < 3.11 \text{ meV}$  only a single edge state away from the window region con-

tributes  $G_0$  to the conductance. In the energy region  $3.11 < E < 3.25$  meV when only one state in the lowest part of the second subband contributes to the conduction there is a stronger backscattering for the smaller window sizes. We have checked this region for even larger window with  $\alpha = 0.0001$  nm $^{-2}$  and find then the strongest backscattering for all our tested values of  $\alpha$ . The reason for the suppressed backscattering at  $\alpha = 0.0002$  nm $^{-2}$  is a formation of a resonance state in the window region for this particular size of it. The electron probability density for this state  $n_i = 1_2$  is seen in Fig. 8. The resonance is in

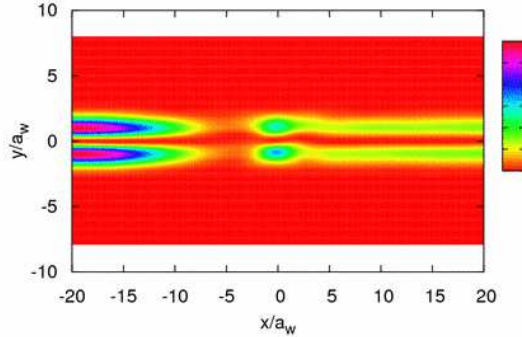


FIG. 8: (Color online) The electron probability density for the mode  $n_i = 1_2$  at input energy  $E = 3.212$  meV,  $B = 0.5$  T,  $\alpha = 0.0002$  nm $^{-2}$ , and  $D = 1.0$  corresponding to the solid red curve in the upper panel of Fig. 5.

some sense opposite to what happens at  $E = 2.902$  meV in Fig. 7(b), since here there is resonant forward scattering from the window region but the backscattered wave tunnels initially into the barrier left of the window. For the same energy the  $n_i = 0_2$  state bypasses the scattering region unperturbed.

In the energy region  $3.25 < E < 3.417$  meV two more states in the second subband can contribute to the conductance and again we have a complex superposition of hole- and electron-like states interacting with the window leading to a conductance minimum for the largest window,  $\alpha = 0.0002$  nm $^{-2}$ . The electron probability density for  $E = 3.417$  meV in the peak at the endpoint of this interval is shown in Fig. 9. In subfigure 9(a) we see the incoming state in the lowest subband bypassing the window unperturbed, but in Fig. 9(b) the  $n_i = 1_2$  hole-like mode undergoes a inter-wire backscattering in the window and we see a faint wave continuing through the wire. In subfigure 9(c) the other hole-like mode  $n_i = 1_4$  shows a quasi-bound state in the window. The interference pattern seen in these two hole-like states indicates a substantial mixing or scattering between them. Some particles coming into the system in the  $n_i = 1_2$  mode leave the system in the  $n_i = 1_4$  mode. The last panel of Fig. 9(d) shows the only incoming electron-like state  $n_i = 1_6$  in the second subband. Clearly the electrons in this mode are not backscattered to any extent, but the

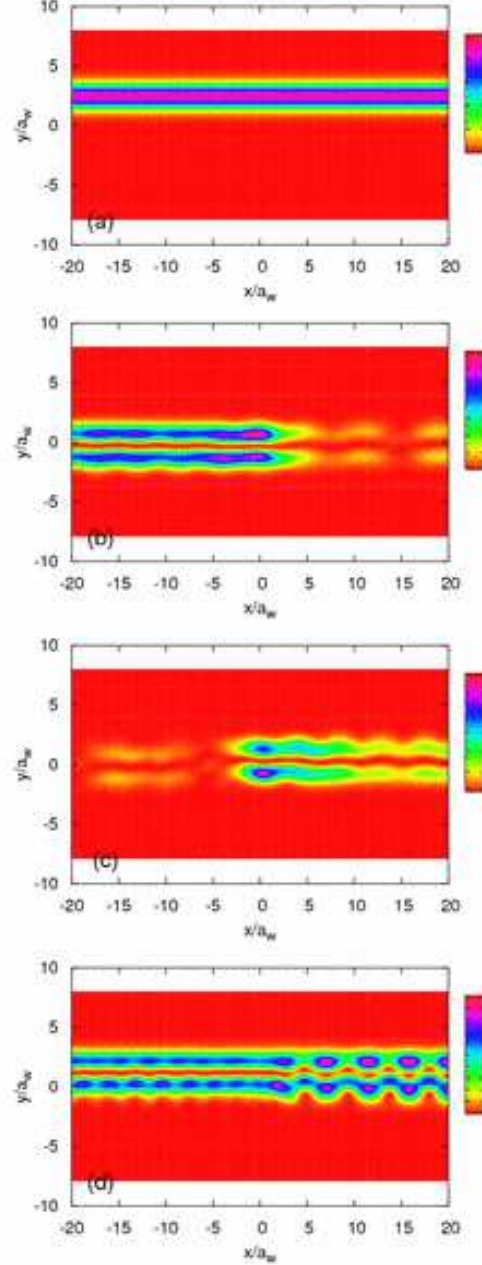


FIG. 9: (Color online) The electron probability density at input energy  $E = 3.417$  meV for mode  $n_i = 0_2$  (a),  $n_i = 1_2$  (b),  $n_i = 1_4$  (c), and  $n_i = 1_6$  (d). See Fig. 6 for the labeling of the modes.  $B = 0.5$  T,  $\alpha = 0.0002$  nm $^{-2}$ , and  $D = 1.0$  corresponding to the solid red curve in the upper panel of Fig. 5.

interference pattern again indicates interference with the two hole-like modes propagating in the same subband.

In the semi-gap energy region  $3.42 < E < 3.79$  meV the two active incoming modes of the lowest two subbands contribute their full share to the conductance unperturbed by the central window, except for a narrow

conductance dip at  $E = 3.761$  meV where the  $n_i = 1_2$  mode interacts strongly with an evanescent state at the bottom of the third subband. The corresponding electron probability is seen in Fig. 10. The breaking of the

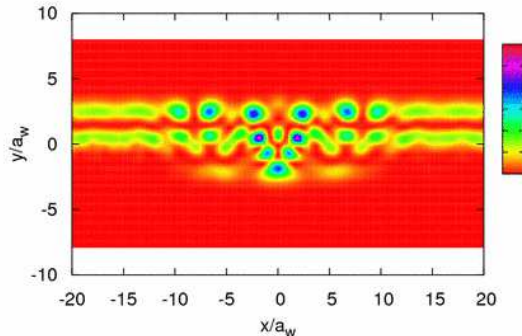


FIG. 10: (Color online) The electron probability density at input energy  $E = 3.761$  meV for mode  $n_i = 1_2$ .  $B = 0.5$  T,  $\alpha = 0.0002$  nm $^{-2}$ , and  $D = 1.0$  corresponding to the solid red curve in the upper panel of Fig. 5.

parity by the magnetic field makes this backscattering through an evanescent state in the next higher subband possible.<sup>7</sup> The resonance state seen in Fig. 10 is an example of persistence of a wave function in an open system, or “scarring of a wave function” discussed by Akis et al.<sup>10</sup>

In the narrow energy range  $3.79 < E < 3.83$  meV two incoming modes are active in the third subband and we have a structure in the conductance similar to what happened around the bottom of the two lower subbands. But in the energy range  $3.83 < E < 4.2$  meV when only one incoming mode exists in the third subband we have a curious “exchange” of backscattering strength between the conduction curves for the longest window and the shorter ones. The strength changes at a resonance caused by an evanescent state at  $E = 4.01$  meV. The character of a close evanescent state changes at this energy, below it is electron-like but above it is hole-like. For the larger window,  $\alpha = 0.0002$  nm $^{-2}$ , the remnant of the resonance enhances conductance above  $E = 4.01$  meV, and has opposite effects for the larger windows.

#### IV. SUMMARY

In this work we have shown that magnetotransport in a lateral double quantum wire system with a window between the parallel wires shows clear fingerprints of the complex subband structure of the system caused by the parity breaking of the perpendicular magnetic field. We have been able to specify regions in the conductance of the system as a function of the incoming energy  $E$  that reflect the underlying electron- or hole-like states active in the transport process both among the propagating and the evanescent modes of the system. This connection of the transport features to the energy spectrum was of course not possible in a single quantum wire with an island in the center of the scattering region creating a short section of a double quantum wire embedded in larger single wire.

An expected simple yet nontrivial result of the complex subband structure for the double wire system is the appearance of irregular steps in the conductance as a function of the energy of the incoming electron wave compared to the regular steps of the single quantum wire of parabolic or hard wall shape.

Here we have selected a shallow window as a particular scattering potential between parallel quantum wires of a particular shape such that the states around subband bottoms are most affected by inter-wire scattering processes. The numerical methods employed using analytical matrix elements allow for a wide variety of wire shape and scattering potentials that can have more effects on edge-like modes of the system.

#### Acknowledgments

The authors acknowledge the financial support by the Research and Instruments Funds of the Icelandic State, the Research Fund of the University of Iceland, and the National Science Council of Taiwan. C.S.T. is grateful to the computational facility supported by the National Center for High-performance Computing of Taiwan.

<sup>1</sup> B.-Y. Gu, C.-R. Huo, Z.-Z. Gan, G.-Z. Yang, and J.-Q. Wang, Phys. Rev. B **46**, 13274 (1992).

<sup>2</sup> C.-S. Tang, W. W. Yu, and V. Gudmundsson, Phys. Rev. B **72**, 195331 (2005).

<sup>3</sup> J. C. Barbosa and P. N. Butcher, Superlattices and Microstructures **22**, 325 (1997).

<sup>4</sup> S. V. Korepov and M. A. Liberman, Phys. Rev. B **60**, 13770 (1999).

<sup>5</sup> S. V. Korepov and M. A. Liberman, Physica B **109**, 92 (2002).

<sup>6</sup> S. A. Gurvitz, Phys. Rev. B **51**, 7123 (1995).

<sup>7</sup> V. Gudmundsson, Y.-Y. Lin, C.-S. Tang, V. Moldoveanu, J. H. Bardarson, and A. Manolescu, Phys. Rev. B **71**, 235302 (2005).

<sup>8</sup> P. F. Bagwell, Phys. Rev. B **41**, 10354 (1990).

<sup>9</sup> S. A. Gurvitz, and Y. B. Levinson, Phys. Rev. B **47**, 10578 (1993).

<sup>10</sup> R. Akis, J. P. Bird, and D. K. Ferry, Appl. Phys. Lett. **81**, 129 (2002).